2011 International Conference on Modeling, Simulation and Control
IPCSIT vol.10 (2011) © (2011) IACSIT Press, Singapore

Linear Unmixing and Target Detection of Hyperspectral Imagery Using OSP

Muhammad Ahmad [1] and Dr. Ihsan Ul Haq[1]

[1]Department of Electronics Engineering, Faculty of Engineering and Technology, International Islamic University, Islamabad (IIUI)-44000, Pakistan

mahmd00@yahoo.com; ihsanasghar2000@yahoo.com

Abstract: Proposed technique of dimension reduction, unmixing and target detection is apparent to implement and compute the results in a very fast and efficient manner. Targets Alunite, Buddingtonite, Calcite, Kaolinite, and Muscovite are detected well and have high spectral similarities. To reducing the computational complexity Standard Deviation with respect to correlation distance ($\mathrm{STD}_{\chi} - \mathrm{COR}$) method is used. Number of end-members is enumerating by orthogonal subspace projection (OSP) method. The expectation maximization framework infers the unmixing matrix. Abundance fractions are modeled as a mixture of density functions and it cannot be unmix easily that is why self iteration method is adopted. A set of tests with real hyperspectral data evaluates the performance and illustrates the effectiveness of the proposed method. The experimental results show the effectiveness of the method on hyperspectral data unmixing. Hyperspectral remote sensing is used in a large array of real life applications e.g. Surveillance, Mineralogy, Physics, and Agriculture. The entire work is done by using MATLAB.

Keywords: Hyperspectral; Dimension reduction; Unmixing; Detection; Pearson correlation.

1. Introduction

Hyperspectral remote sensing is the exact tool for increasing knowledge and perceptive of the earth's surface. Hyperspectral imaging is anxious with capacity, examination, and analysis of the spectra acquired from a given sensor at a short, medium or long distance by an air-borne or satellite [1]. NASA's Jet propulsion Laboratory (JPL) began a revolt in remote sensing by developing new instruments such as the air-borne imaging spectrometer. This concept of hyperspectral imagery was bigning in the 1980's by A. F. H. Goetz and his colleagues at NASA's [1]. This was used more than 200 spectral bands and able to cover the wave-length region from $0.4 - 2.5$ μm at nominal spectral resolution of 10 μm. Hyperspectral remote sensors collects concurrently image data in dozens or hundreds slight and neighboring spectral bands over wave-length that can range from the close to ultraviolet through the thermal infra-red at resolution of fine 10 μm.

Hyperspectral system produces a substantial amount of data. The measurements make it feasible to drive a continuous spectrum for each image cell. These images spectra can be compared with the field or laboratory reflectance spectra in order to recognize and map surface materials such as particular types of vegetations or diagnostic minerals associated with ore deposits. The radiance acquired by hyperspectral sensors cannot be directly compared with the spectral library radiance or even any other radiance data sets. It is just because of the atmospheric effects and illuminations. To overcome this problem, transform the radiance spectra into the reflectance which make atmospheric correction. Hyperspectral data enables the analysis to detect more materials, objects, and regions of interest with more accuracy than previously possible. The science of remote sensing has advanced over the past years by using progressively more capable sensors.

+ Corresponding author. Muhammad Ahmad, Tel.: + (+92-321-6617922);
E-mail address: mahmad00@yahoo.com .

Hyperspectral data Dimensional Reduction, Unmixing and Target Detection problem is addressed in this article. Decomposition of pixel spectrum into the collection of spectral signatures and corresponds their abundance fractions is called the hyperspectral unmixing. The spectral resolution with spatial resolution can be changed by unmixing.

Data reduction is a consequence of the fact that the number of end-members presents in the scene is usually much smaller than the number of bands. Dimensional reduction is reduce the computational complexity and improves the signal to noise ratio. Therefore reducing the dimensionality without missing important information is very important issue for remote sensing community. Dimensional reduction is categorized in two ways: Feature Extraction is done by mapping the correlation of high dimensional data onto uncorrelated low dimensional data. Feature Selection is usually carried out the original feature space; these techniques do not alter the original representation of the variables but merely select a subset of them. There is no need of any transformation while selecting a subset of features for dimensional reduction, but the main focus on selecting features among the existing features.

Unmixing of hyperspectral data is usually carried out the two steps. First is to estimates the spectral signatures of the different end-members and second is to find the abundance fractions of each end-member. To perform the hyperspectral unmixing and target detection procedure, a mixture model must be adopted either linear or non-linear mixture model. In our proposed work a linear mixture model used and described below. To illustrate this, assume that a linear combination of $\bar{S}_i = [\vec{S}_1\ \vec{S}_2 \ldots \vec{S}_i]$ signatures and their corresponding abundance fractions $\vec{A}_i = [a_1\ a_2\ \ldots\ a_i]^T$, i = 1, 2… K. where K is total number of targets and L is total number of bands. Thus

$$\vec{X}_i = \bar{S}\,\vec{A} + \vec{W} \tag{1}$$

Where W is an additive white Gaussian noise. The mixing matrix $\bar{S}$ can be inferred if the columns of $\bar{S}$ are linearly independent, than $\vec{A}$ can be computed and thus the materials can be resolved within pixel without increasing the spectral resolution. A necessary condition for the columns of $\bar{A}$ to be independent is $L \geq K$.

2. Problem Statement

Our main focus and attention is to enhance the results of hyperspectral dimensional reduction, unmixing and target detection accuracy by using statistical constraints. The emergence of image data with large number of spectral bands has presented image processing and interpretation challenges yet they not experienced with hyperspectral data sets. There is a need to develop the data reduction, unmixing and detection methods to utilize the maximum amount of information and reparability that hyperspectral images data offers while simultaneously avoiding the difficulties inherent in hyperspectral space.

2.1 Dimensional Reduction

Suppose that hyperspectral data contains $\{\bar{X}_i\}_{i=1}^{L}$ band images and $\widetilde{STD}_i$ is the standard deviation of i^{th} band image. Then we have [2]

$$\bar{X}_i = \left(\frac{1}{MN}\sum_{i=1}^{MN}\left(b_i - \widetilde{STD}_l\right)^2\right)^{\frac{1}{2}} \tag{2}$$

Where MN is total number of pixels in each band image, $\bar{X} = [\vec{x}_1, \vec{x}_2 \ldots \vec{x}_n]$, the distance between the vectors $[\vec{x}_r]$ & $[\vec{x}_s]$ is defined as [3],

$$X_{rs} = 1 - \frac{(x_r - \bar{x}_r)\,(x_s - \bar{x}_s)^T}{[(x_r - \bar{x}_r)\,(x_r - \bar{x}_r)^T]^{\frac{1}{2}}\,[(x_s - \bar{x}_s)\,(x_s - \bar{x}_s)^T]^{\frac{1}{2}}}$$

The result from above L band images is given as $\bar{X} = [\bar{X}_i]_{i=1}^{L}$ [3-4] and also selected bands are shown in Figure 1.

2.2 Proposed Method for Unmixing

Presume that $\overline{X} = \bar{r} + \overline{W}$, here $\bar{r}$ is a data matrix of size (L x M) and $\overline{W}$ is a white noise matrix, where L is total number of bands and M is total number of pixels in data. The projecting matrix is estimated as,

$$\alpha(\bar{r}) = \sum_{i=1}^{L}\left[\left(\frac{[\vec{r}_i - E[\vec{r}_i]]}{M}\right)\right]; \quad \beta(\bar{r}) = \left(\sqrt[1/2]{(S(\vec{r}_i))}\right) \text{ so } \bar{\rho}_{\bar{r}} = \frac{\alpha}{\beta}$$

The Eigen value decomposition of projecting matrix is found as,

$$\bar{r} = \overline{U}\,\overline{\sum}\,\overline{U}^T$$

Here $\overline{U}$ is the Eigen values matrix and $\overline{\sum}$ is a diagonal matrix having real diagonal elements λ_i such that $\lambda_1 \geq \lambda_2 \geq \lambda_3 \geq \cdots \lambda_{\min(l,m)} \geq 0$. Since $\lambda_i$are the singular values of $\overline{U}$ and the first $\min(m, n)$ columns of $\overline{U}$ and $\overline{U}^T$ are the left and right singular vectors of $\overline{U}$. Since $\overline{P}$ is the projected matrix onto Eigen values matrix $\overline{U}$.

$$\overline{P} = \overline{U} * \overline{U}^T \tag{4}$$

Since the mean of the data matrix and projection matrix is estimated as

$$E[\bar{x}] = \frac{1}{N}\sum_{i=1}^{N}\vec{x}_i$$

$$E[\bar{r}_W] = \frac{1}{N}\sum_{i=1}^{N}\vec{r}_{W_i}$$

So the order of data is defined as, ε is a scaling factor,

$$K = \ \text{argmin}\left\{\varepsilon * \text{trace}\left(\overline{U} * \bar{\rho}_{\bar{r}_W}\right) - \left(\text{trace}\left(E[\bar{x}] * \overline{U} * E[\bar{x}]^T\right)\right)\right\}$$

The subspace of data can be found as [4-5], and this part is a back bone of our work.

$$\bar{r}_k = I - \overline{U} * \overleftrightarrow{(\overline{U}^T * \overline{U})} * \ \overline{U}^T$$

$$\overline{X} \ = \ \bar{r}_k * \bar{r}$$

Where $\overleftrightarrow{(\overline{U}^T * \overline{U})}$ is the pseudo inverse of $\overline{U}$.

$$\hat{\overline{A}}_k = \left(\overline{U}_i * \left(\hat{\bar{\alpha}}_k - \hat{\bar{\beta}}_k\right)\right)$$

Hence the mixing matrix is found as $\overline{S} \ = \ \overline{X} * \ \overline{A}^{-1}$ and since abundance fractions are modeled as a mixture of source densities, so it cannot be unmixed easily, so for this we used self iteration method. The unmixing matrix infer by using the expectation maximization algorithm [6].

3. Results

In the presented research work, a sub image of size 350×350 with 224 bands of a data set taken on the AVIRIS flight [7] has been used and shown in Figure 2 A, and the laboratory end-members signatures for 189 bands are predominantly of Alunite-AL706NA, Buddingtonite-NHB2301, CalciteCO2004, KaoliniteKGa1wxl, and Muscovite-GDS108 are shown in Figure 2 B. The instrument of AVIRIS covers 0.41 – 2.45 μm regions in 224 bands with a 10 nm bandwidth and flying at an altitude of 20 km, it has an Instantaneous field of view (IFOV) of 20 m and views a swath over 10 km wide. Prior to the analysis of AVIRIS Cuprite image data, low SNR bands 1 – 3, 105 – 115 and 150 – 170 have been removed and the remaining 189 bands are used for experiments. Preserving the maximum information, the number of bands required are 22.

The found and laboratory end-members signatures are predominantly of Alunite AL706NA and Buddingtonite NHB2301 are shown in Figure 3 (A-B). The ground truth spectral coordinates are **161-62; 234-209; 347-30; 298-22; 271-33**. The 3-dimensional visualization of the end-members abundance fractions shows in Figure 4 (A-C). Since the detected end-members shows high similarity among the same end-members. The spectral angles between found and actual signatures of predominantly Alunite-Alunite, Buddingtonite-Buddingtonite, Calcite-Calcite, Kaolinite- Kaolinite, and Muscovite-Muscovite are as follows **0.048636, 0.035872, 0.029117, 0.058609, and 0.039505.** The product matrix M-est of mixing matrix and M is identity in an ideal scenario but obtained in our case is given at the end of the results corresponding for all five

minerals namely Alunite AL706NA, Buddingtonite NHB2301, CalciteCO2004, Kaolinite KGA1-WX1, and Muscovite GDS108.

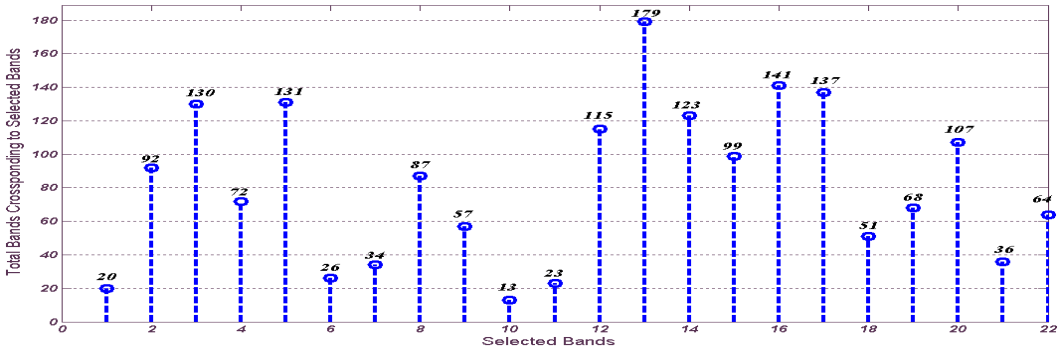

Figure 1: Selected Bands

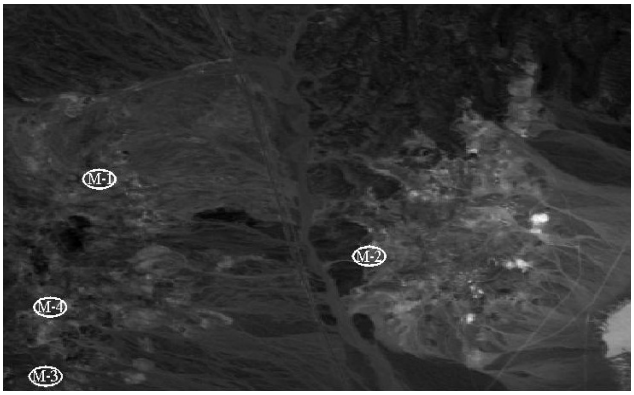

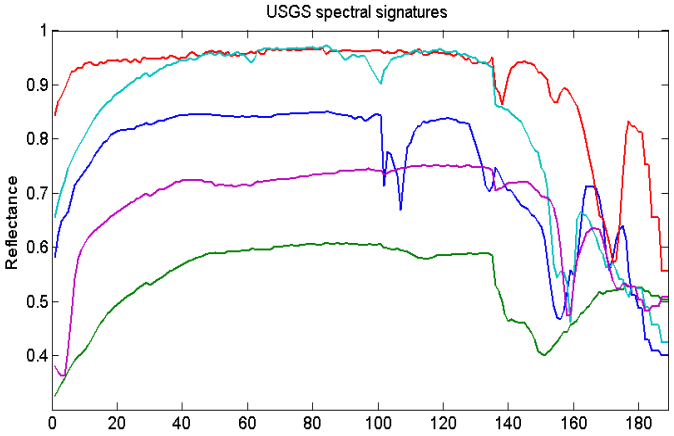

Figure 2 A: 20th Band of Cuprite image: Ground truth spectral positions of four minerals

Figure 2 B: USGS spectral signatures of Alunite-AL706NA, Buddingtonite-NHB2301, CalciteCO2004, KaoliniteKGa1wxl, and Muscovite-GDS108 for 189 bands.

$$\mathbf{M_{EST}} = \begin{bmatrix} \mathbf{0.9995} & \mathbf{-0.0004} & \mathbf{-0.0006} & \mathbf{-0.0006} & \mathbf{-0.0005} \\ \mathbf{-0.0007} & \mathbf{0.9995} & \mathbf{-0.0008} & \mathbf{-0.0008} & \mathbf{-0.0006} \\ \mathbf{-0.0008} & \mathbf{-0.0006} & \mathbf{0.9991} & \mathbf{-0.0009} & \mathbf{-0.0007} \\ \mathbf{0.0001} & \mathbf{0.0001} & \mathbf{0.0001} & \mathbf{1.0001} & \mathbf{0.0001} \\ \mathbf{0.0000} & \mathbf{0.0000} & \mathbf{0} & \mathbf{0.0000} & \mathbf{1.0000} \end{bmatrix}$$

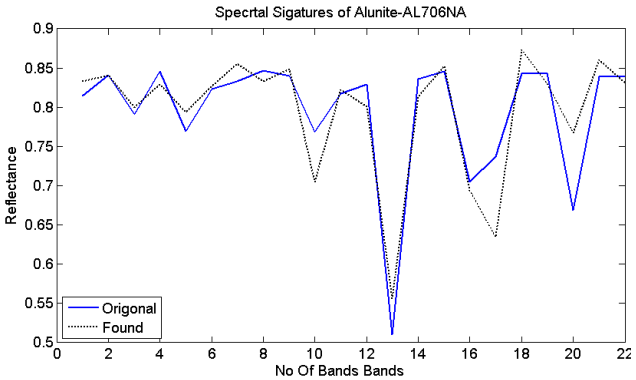

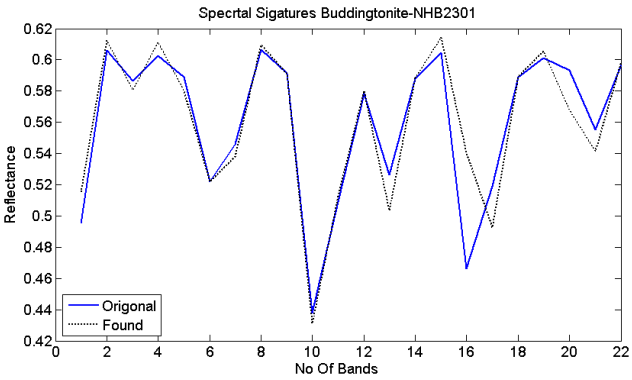

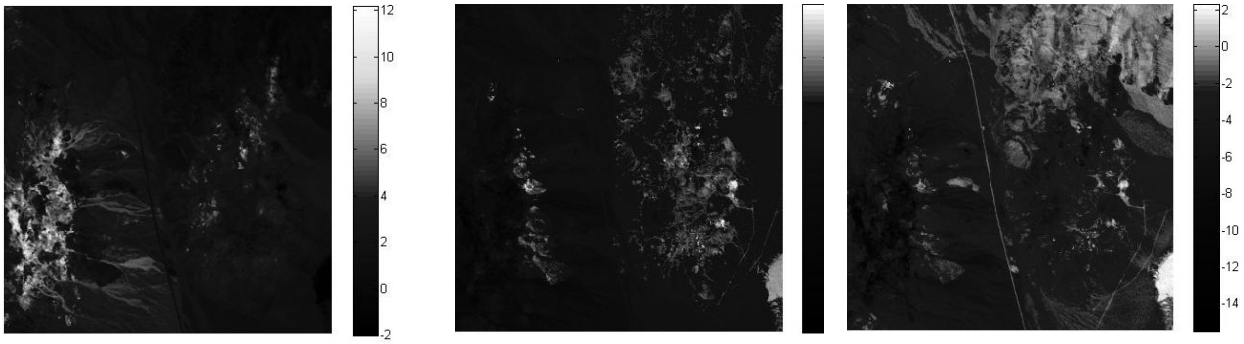

Figure 4 (A-C): 3-Dimensional visualization of spectral signatures for Alunite-AL706NA, Buddingtonite-NHB2301, and Muscovite-GDS108.

4. Conclusion

The end-members are detected well and have high spectral similarities. The total CPU processing time for both subspace estimation by OSP, Unmixing, and end-members detection is 35.297 seconds on Intel core i-7 processor. OSP method is used for estimating the subspace, which spans the original space. The whole work is done by using MATLAB. Here one thing is to be noted that this method is only for reduced hyperspectral data (22 bands) not for full bands (189 bands). This method is approximately perfect for 22 bands.

5. Acknowledgements

I owe my things to the work of "H. Ren, J. C. Harsanyi and C.-I. Chang," which opened a new vista of research for me in field of remote sensing. I drew tremendous assistance from there papers. My paper is as a matter of fact sequel to their diligent task they carried out in the field of Hyperspectral imaging. I would like to express my thanks to NASA's which provided research data for my prompt utilization. I am really very grateful to my supervisor for his timely help in the completion of my work. I am also feeling obliged to my friends without their help I would have not accomplished my research objectives.

Finally I owe my achievement to the efforts of my family particularly my parents and brothers (Khalid Omar, Abid Omar and Asif Omar) without their best wishes success would have been distant thunder.

And above all, to the Almighty God, who never cease in loving us and for the continued guidance and protection.

6. References

[1] A. F. H. Goetz, G. Vane, J. Solomon, and B. Rock, "Imaging spectrometry for earth remote sensing", in Airborne Imaging Spectrometer Data Analysis workshop, JPL Publication, vol. 228, pp. 22-29, 1985.

[2] Muhammad Sohaib, Ihsan-Ul-Haq, Qaisar Mushtaq, "Dimensional Reduction Of Hyperspectral Image Data Using Band Clustering And Selection Based On Statistical Characteristics Of Band Images", IEEE International Conference on ICIIT, Proceedings, 2010.

[3] Muhammad Ahmad, Dr. Ihsan Ul Haq, Qaisar Mushtaq and Dr. K.A.Bhatti "A new Statistical approach for band clustering and band selection using K-means clustering", not published but submitted to journal, May 2011.

[4] H. Ren and C.-I. Chang, "Automatic spectral target recognition in hyperspectral imagery", IEEE Transactions on Aerospace and Electronic Systems, vol. 39, no. 4, pp. 1232–1249, 2003.

[5] J. C. Harsanyi and C.-I. Chang, "Hyperspectral image classification and dimensionality reduction: An orthogonal subspace projection," IEEE Transactions on Geo science and Remote Sensing, vol. 32, no. 4, pp. 779–785.

[6] Muhammad Ahmad, Dr. Ihsan Ul Haq, Qaisar Mushtaq and Dr. K.A.Bhatti, "Hyperspectral Data Dimensional Reduction and Source Separation Using MAD and Maximum Log-Likelihood", not published but submitted to journal, June 2011.

[7] G. Vane, R. Green, T. Chrien, H. Enmark, E. Hansen, and W. Porter, "The airborne visible/infrared imaging spectrometer (AVIRIS)," Remote Sensing of the Environment, no. 44, pp. 127–143, 1993.